

Article

Molecular Cartography of a Hawaiian Coral Assemblage

Joseph W. P. Nakoa III^{1,2}, John H. R. Burns^{2,3} , Kanoelani Steward^{2,3,4}, Lauren M. Kapono^{2,3,4}
and Clifford A. Kapono^{2,5,*}

¹ School of Life Sciences, Arizona State University, Tempe, AZ 85281, USA

² MEGA Lab, Hilo, HI 96720, USA

³ Marine Science and Data Science, University of Hawai'i at Hilo, Hilo, HI 96720, USA

⁴ Nā Maka o Papahānaumokuākea, Kamuela, HI 96743, USA

⁵ School of Ocean Futures, Arizona State University, Tempe, AZ 85281, USA

* Correspondence: ckapono@asu.edu

Abstract: Coral reefs are declining due to multiple factors including overfishing, anthropogenic pollution, and ocean acidification. Diseases affecting corals have increased in recent decades, yet the etiology of nearly all diseases remains poorly understood. Here, we investigated three-dimensionally mapped molecules and microbes from healthy and diseased coral tissue sampled across the landscape of a coral assemblage at the Wai'ōpae tide pools, Southeast Hawai'i Island. A 3D molecular cartographic platform was used in combination with molecular networking tools to characterize healthy coral tissue and tissue affected by the disease growth anomaly (GA). Tissues of healthy *Montipora flabellata* and *Montipora capitata* exhibited higher microbial diversity compared to *Porites lobata* and GA-affected *M. capitata* corals. Increases in relative abundance of *Ulvophyceae* and sterols were observed in GA lesions, while chlorophyll decreased. Conversely, healthy coral tissues were characterized by the presence of cyanobacteria in the order of Stramenopiles, in addition to higher relative chlorophyll levels. Leveraging innovative molecular cartography provides new insight into molecular characteristics of coral colonies, and helps to better understand how diseases affect the molecular landscape of corals.

Keywords: 3D cartography; photogrammetry; metabolomics; microbiome; coral reef



Citation: Nakoa, J.W.P., III; Burns, J.H.R.; Steward, K.; Kapono, L.M.; Kapono, C.A. Molecular Cartography of a Hawaiian Coral Assemblage. *Diversity* **2023**, *15*, 1061. <https://doi.org/10.3390/d15101061>

Academic Editor: Bert W. Hoeksema

Received: 31 August 2023

Revised: 26 September 2023

Accepted: 26 September 2023

Published: 3 October 2023



Copyright: © 2023 by the authors. Licensee MDPI, Basel, Switzerland. This article is an open access article distributed under the terms and conditions of the Creative Commons Attribution (CC BY) license (<https://creativecommons.org/licenses/by/4.0/>).

1. Introduction

As diseases continue to threaten coral reef ecosystems in conjunction with local and global stressors, there is a pressing need to develop tools that better characterize the biology and ecology of corals [1,2]. The coral holobiont is a complex assemblage of diverse organisms including the mutualistic dinoflagellate genus, *Symbiodinium*, and associated bacterial, archaeal, viral, and other eukaryotic microorganisms [3]. Advances in culture-independent microbial analysis has enabled investigators to characterize the microbial community of the coral holobiont, although fully understanding the functional role coral microbiomes play in the epizootiology of coral health remains challenging [3–6]. Additionally, recent advances in liquid chromatography tandem mass spectrometry (LC-MS/MS) molecular profiling have enabled scientists to characterize coral metabolomes with increased sensitivity and reproducibility [7–10]. Leveraging advanced technologies will be critical for identifying components of the coral microbiome that influence host resistance and resilience to disturbance and disease. Recent research has primarily focused on the role of microbiomes in coral health resilience, but despite the improvements in molecular research techniques, there has been minimal improvement to our mechanistic understanding of how external stressors influence the coral microbiome, and in turn the host physiology [3,11]. More research is needed to determine microbiome characteristics associated with coral host conditions to develop tools and biomarkers for assessing coral health prior to the manifestation of disease [3].

Structure-from-Motion (SfM) photogrammetry techniques are capable of producing high-resolution three-dimensional (3D) reconstructions of underwater coral reef habitats [12–15]. The resulting 3D models can be visually and structurally analyzed to enhance ecological studies investigating the spatial and structural dynamics of coral communities [12–16]. The models are also capable of being annotated to both visualize and analyze data onto the reconstructed reef habitat [16]. Innovative 3D cartography tools can be used to annotate and map sampling locations onto 3D reconstructions to visualize the expression of molecular data products across reef landscapes [17]. Few studies have applied these approaches on coral reefs. This study integrated molecular data derived from coral samples onto high-resolution 3D reconstructions of a coral assemblage to conduct molecular profiling and examine patterns in microbial and metabolite features associated with coral taxonomy and health conditions.

The Wai'ōpae coastline was located at the southeastern tip of Hawai'i Island prior to being covered by the 2018 lower Puna eruption. Since the formation of Wai'ōpae during the 1960 Kapoho eruption, it supported a high abundance and diversity of coral in a network of submerged pools formed by permeable basalt substrate [18]. Before being lost, Wai'ōpae received a high frequency of natural and anthropogenic disturbances, both chronic and acute [19,20]. Coral Growth Anomaly (GA) is a prominent disease affecting corals throughout the global oceans, and exhibits an abnormally higher prevalence at Wai'ōpae than any other sites surveyed throughout the Hawaiian Archipelago [19,20]. Little is known about the etiology of GA and few studies have investigated the molecular underpinnings of this disease [21].

Three-dimensional reef mapping and genomic analyses have been performed independently to investigate coral communities at Wai'ōpae, yet no studies have examined the 3D distribution of molecules on coral colonies at this site [14,21,22]. Moreover, this study employs a novel approach of combining molecular and photogrammetry tools to enable 3D molecular cartography on an assemblage of coral colonies [23]. The 16S rRNA gene amplicon sequencing and LC-MS/MS data were mapped onto a high-resolution 3D reconstruction of a Hawaiian coral assemblage composed of *Porites lobata*, *Montipora capitata*, and *Montipora flabellata* species (Figure 1). Samples were collected along spatial gradients where the coral colonies physically interacted, and also along gradients where tissue was affected by GA disease. Sampling along gradients where adjacent colonies were physically contacting one another provides a means to assess possible patterns in molecular profiles associated with competitive interactions between corals. Analyzing competing corals from two separate genera, different species from the same genera and from the same species can shed light on how competition interactions affect coral biology. This study identified unique molecular features that distinguish each coral species as well as molecular features associated with GA-affected coral tissue. Analyzing the data across the landscape of the 3D-reconstructed coral assemblage provides a new and useful perspective for determining spatial patterns in molecular profiles. This approach can be scaled up to determine molecular underpinnings that drive biological responses and ecological characteristics in coral communities at other locations.

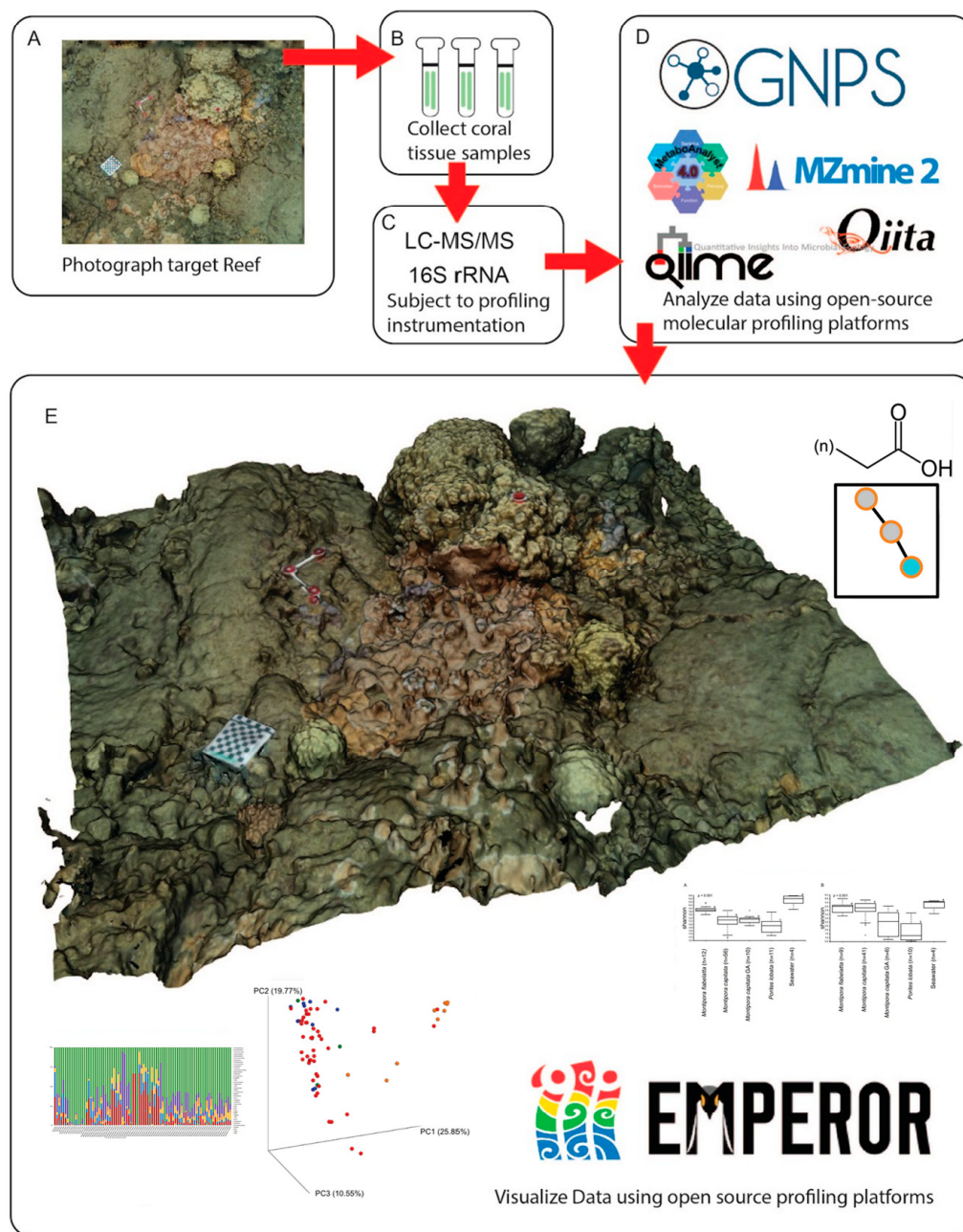


Figure 1. Flowchart of 3D multi-omic profiling protocol. (A) Coral samples were collected and overlapping images of the coral assemblage were taken from oblique and planar angles. Agisoft Photoscan was used to create a 3D model of the coral assemblage and sampling coordinates were annotated using Geomagic Wrap software [24,25]. (B) Extractions were performed for both LC-MS/MS and 16S rRNA gene amplicon (“16S”) molecular profiling, using the V4 region according to the Earth Microbiome Project protocols [26,27]. (C) Samples were subjected to LC-MS/MS and 16S sequencing. (D) Raw mass spectra and sequencing outputs were converted and assembled to mzXML and FASTQ formats, respectively. Global Natural Products Social Molecular Networking (GNPS), Metaboanalyst, MZmine 2, Qiita, and QIIME software were used to process data [28–31]. (E) Visualization was performed in the ‘ili, EMPeror, Cytoscape, Qiita, and Metaboanalyst graphical user interfaces [17,32–34].

2. Methods

2.1. Coral Tissue Sampling

A total of 83 samples were collected from coral colonies and the surrounding seawater at Wai'ōpae (19°29'55" N, 154°49'06" W), Southeast Hawai'i Island, in accordance with traditional Hawaiian gathering protocols and State of Hawai'i guidelines (DAR permit number 53929). Tissue samples were collected with a 1 cm core from *P. lobata* (n = 11), *M. flabellata* (n = 12), and *M. capitata* (n = 56) corals (Figure A1). The colonies in this assemblage all interacted along their borders and samples were taken along spatial gradients perpendicular to the colony borders. A number of tissue samples from *M. capitata* were collected from tissue affected by growth anomalies (n = 10) and non-GA tissue (n = 10) within 3 cm of the GA lesions. GA lesions were characterized as having reduced polyp and tuberculae densities compared to healthy *M. capitata* tissue [19]. Moreover, 1.5 mL water samples (n = 4) were taken just above the coral surface. The location of each sample was recorded by photographs and video for later annotation at precise locations to the pixel coordinates on the corresponding 3D reconstruction. Each sample was subjected to molecular profiling by mass spectrometry and DNA sequencing. Samples were flash-frozen with liquid nitrogen and shipped overnight under dry ice to the University of San Diego, California. Samples were stored at −80 °C until extraction.

2.2. Three-Dimensional Reconstruction of Coral Assemblage

Images, prior to sampling, were collected using methods developed specifically for reconstructing a 3D map of the coral reef habitats that were sampled [14]. One coral assemblage was identified that contained several corals with interacting borders of different genus (*Porites/Montipora*), same genus different species (*M. capitata/M. flabellata*), same species (*M. capitata/M. capitata*), and diseased tissue (*M. capitata* GA). Ground control points (GCPs) were placed at the corners of the coral assemblage with known x, y, z coordinates to enable precise spatial rectification for the resulting 3D models. A calibration grid and a scale marker were placed at the border of the survey area to validate spatial accuracy. Overlapping photographs were taken from planar and oblique angles while swimming above the coral assemblage in a boustrophedonic pattern. All photos were taken with a Canon 5D Mark III digital SLR camera with a 24–70 mm lens set at 24 mm (Canon USA Inc., New York, NY, USA) in an Ikelite housing with an 8 in. hemispheric dome port (Ikelite Underwater Systems, Indianapolis, IN, USA). The 8 in. hemispheric dome port significantly reduces distortion due to refraction and improves the ability of the software to accurately calibrate and align the images [35,36].

Three-dimensional reconstructions of the coral assemblage were rendered using Agisoft modeling software (Agisoft LLC., St. Petersburg, Russia). Images were uploaded into the PhotoScan software and camera calibration was performed using Brown's distortion model. PhotoScan aligned all overlapping images using algorithms that detect invariant features from the overlapping image sequences. The invariant features were then used to create geometrical projective matrices and determine the exact position and orientation of the camera for each sequential image [16]. Three-dimensional geometry was constructed on the 2D image plane using the extrinsic parameters, which define the location and orientation of the camera reference frame with respect to a known world reference frame and in conjunction with the intrinsic parameters, which link the pixel coordinates of an image point with the corresponding coordinates in the camera reference frame. Iterative bundle adjustments were used to refine the 3D coordinates of the scene geometry and minimize reprojection error in order to create a sparse 3D point cloud that accurately represented the structure of the photographed coral reef plot. Markers were digitally annotated onto each of the GCPs using the PhotoScan software, and the known x, y, z values of the GCPs were used to optimize the alignment of the photos and to ensure that the resulting models were spatially rectified. After the initial point cloud was optimized, a dense point cloud was generated and used to construct a continuous mesh surface that was then triangulated and rendered with the sequential images to create textured 3D digital surface models

representing the coral assemblage at Wai'ōpae. The 84 coordinates were annotated onto the 3D model in GeoMagic 3D annotation software that represented the actual sampling sites where tissue samples were taken from each coral [37]. Coordinates were matched with each sample file from LC-MS/MS and 16S OTU feature tables.

2.3. Molecular Extraction and LC-MS/MS

Molecular extraction was performed on the frozen samples to capture small molecules that can be subjected to LC-MS/MS. Each sample was lyophilized, weighed, and subjected to 1.0 mL/mg with 70% methanol for 4 h in 10 mL glass vials [38]. The absorbed material was extracted in 500 µL of 50:50 ethanol/water (for mass spectrometric analysis). Supernatant was removed and dried until LC-MS/MS data acquisition.

Molecules were separated using chromatography and detected using a mass spectrometer. Processed coral extracts (5 µL) were subjected to UHPLC chromatographic separation using an UltiMate 3000 UHPLC system (Thermo Fisher Scientific, Waltham, MA, USA), controlled by Chromeleon software (Thermo Scientific). Chromatographic separation was achieved using an 1.7 micron C18 (50 × 2.1 mm) Kinetex UHPLC column (Phenomenex) at 40 °C, using a flow rate of 0.5 mL/min. A linear gradient was used for the separation: 0–0.5 min 5% B, 0.5–8 min 5%B–99%B, 8–9 min 99%B, 9.01–10 min 1%B, 10–10.5 min 5%B–99%B, 11–11.5 min 99%B–1%B, 12–12.5 min 1% B where solvent A is water 0.1% formic acid (*v/v*) and solvent B is acetonitrile with 0.1% formic acid (*v/v*). Column eluent was introduced directly into a Bruker Daltonics maXis Impact quadrupole-time-of-flight mass spectrometer equipped with an Apollo II electrospray ionization source and controlled via otof Control v3.4 (build 16) and Hystar v3.2 software packages (Bruker Daltonics, Billerica, MA, USA). The maXis instrument was first externally calibrated using ESI-L Low Concentration Tuning Mix (Agilent Technologies, Santa Clara, CA, USA) prior to initiation of the sequence of samples, and hexakis (1H,1H, 2H-difluoroethoxy) phosphazene (Synquest Laboratories, Alachua, FL, USA), *m/z* 622.0295089613, was continuously introduced as an internal calibrant (lock mass) during the entirety of each LC/MS run. Data was collected in positive ion mode, scanning from 80–2000 *m/z*. Instrument source parameters were set as follows: nebulizer gas (Nitrogen) pressure, 2 Bar; Capillary voltage, 4500 V; ion source temperature, 200 °C; dry gas flow, 9 L/min. MS1 spectral acquisition rate was set at 3 Hz and MS/MS acquisition rate was variable (5–10 Hz) depending on precursor intensity. Data-dependent MS/MS acquisition was programmed to the top five most intense precursors per MS1 scan and any precursor was actively excluded for 1 min after being fragmented twice. Each MS/MS scan acquired was the average of 4 collision energies, paired optimally with specific collision RF (or “ion cooler RF”) voltages and transfer times in order to maximize the qualitative structural information from each precursor. The auto-acquisition of MS/MS spectra was carried according to specific settings. Precursor *m/z* 100, 300, 500, 1000 was selected; with an isolation width of 2, 4, 6, and 8; with a base collision energy (eV) of 10, 25, 30, 50; a sampled collision energy of (5, 10, 15, 20), (12.5, 25, 37.5, 48), (15, 30, 45, 60), (25, 40, 75, 100); a collision RF (Vpp) of 250, 500, 1000, and 1500 for all precursors; and a transfer time (µsec) of 50, 75, 100, and 150 for all samples was used, respectively.

2.4. Microbial DNA Extraction and Sequencing

DNA extraction was performed on the frozen samples using the Qiagen® MagAttract® PowerSoil® DNA KF kit following the Earth Microbiome Project (EMP) high-throughput DNA extraction protocol to capture microbial DNA from each sample that can be subjected to sequencing [26,27]. Extractions followed manufacturers protocols, with an added 10 min water bath incubation at 65 °C after Lysis buffer addition and retention of the 10 min incubation at 4 °C after lysate addition to IR solution [26]. Extracted DNA from samples was stored at –80 °C until amplification and sequencing.

Extracted DNA was amplified following the EMP protocols adapted for the Illumina MiSeq platform [39]. The V4 region of the 16S rRNA gene was amplified with region-specific primers, including Illumina flowcell adapter sequences [39]. Amplified DNA was

confirmed on agarose gel and quantified using the Quant-iT PicoGreen dsDNA Assay Kit and cleaned using MoBio UltraClean PCR Clean-Up Kits following the manufacturers protocols.

Amplified DNA was diluted to 2 nM in a serial dilution and then balanced with 15–30% PhiX to reduce bias in samples [39]. Samples were then subject to V4 paired-end sequencing following the Earth Microbiome Project Protocols for Illumina MiSeq (University of San Diego, La Jolla, CA, USA) to determine which bacteria were present in each sample [27,39]. Amplicon sequences were demultiplexed and quality-controlled using the defaults provided by QIIME 1.9.1.

2.5. Data Processing

Raw MS data were converted to .mzXML formatting using Bruker Data Analysis 4.1 software and uploaded into MZmine 2.31 [30,33]. Peak detection thresholds for MS1 and MS2 were set at 5.0E3 and 1.0E3, respectively. Chromatogram builder thresholds were set at a minimum height of 1.0 E4 with an isolation tolerance of 0.01 min and m/z tolerance of 20 ppm. Chromatogram deconvolution was performed with a minimum peak height of 3.0 E3 and a peak duration tolerance of 0.1–1 min. MS2 scan pairing was performed at 0.01 da and RT scan pairing was performed at 0.4 min. Chromatograms were deisotoped with a RT tolerance of 0.2 min, an m/z tolerance of 20 ppm, and selected to have a maximum charged state of $[M+2H]^{2+}$. Peaks were aligned with up to a 20 ppm error, with 75% of the alignment priority given to m/z accuracy and 25% to 0.5 min RT overlap. Gap-filling was performed, allowing for a 10% intensity tolerance, a 20 ppm m/z tolerance, and a 0.4 min RT tolerance. Lastly, duplicate peak filtering was performed with a m/z tolerance of 0.01 da and a RT tolerance of 10 min. Aligned peaks were exported as .csv files and .mgf files for further analysis.

2.6. Data Analysis

Principal coordinate analyses (PCoA) were conducted using Bray–Curtis measures of dissimilarity for the metabolomic data. HCA grouping methods were applied to identify clusters among the various tissue samples. Probabilistic quotient normalization of 30% of the samples was used. Plots were visualized in Emperor [32]. PCoA plots for microbiome datasets were constructed in Qiita by using the processed untrimmed 100 rarefied sample set. Ordinates were directly observed on the Qiita interface. Alpha diversity experiments were also performed and observed in Qiita using the untrimmed Wai'ōpae BIOM table rarefied to 100. An adonis PERMANOVA analysis was performed using the vegan package in R studio [40]. Random forest analysis of both the MZmine output data and Qiita OTU feature table was performed in Metaboanalyst to identify top features that describe the metabolome and microbiome species variation [29,41,42]. Peak intensity tables were uploaded and normalized by sum and by mean intensity values. Sum normalization was performed on each sample and mean-centered data scaling was also performed.

Global Natural Products Social Molecular Networking was used to identify MS/MS spectral matches of molecular features in each sample set [28]. Parameters for creating molecular networks include a parent mass tolerance = 0.1 Da, Min matched Peak = 6, Ion Tolerance = 0.5, and Score Threshold = 0.70 with default advance and filter search options. Using these parameters, 64,804 MS/MS spectra were merged into 5006 nodes.

Molecular feature visualization was performed to visualize microbiome and metabolome features on a 3D coral model. The open-source web application 'ili was used by incorporating feature-finding tables and STereoLithography (.stl) file, OBJ 3D file (.obj), and Material Library File (.mtl) created in Photoscan [31].

3. Results

3.1. Metabolomic Profiling:

LC-MS/MS data were subjected to molecular networking into GNPS and visualized in Cytoscape [34]. Using the networking parameters described in the methods, 64,804 spectra

were considered to create nodes or unique molecular ions based on their MS/MS fragmentation patterns (Figure 2). Of the 5006 nodes, 205 (4%) had matching fragmentation patterns (min match peak = 4, cos score = 0.70) to the GNPS reference library and were issued level two or three annotations in accordance with the 2007 metabolomics standard initiative [43]. GNPS provided an estimated FDR value of 1% for annotations above 0.63 cos score value [44,45]. Unannotated nodes are colored in gray. Node borders were colored based on their origin. A majority of the detected nodes were unannotated and shared among the different corals, as indicated by the gray nodes with a dark orange border (Figure 2).

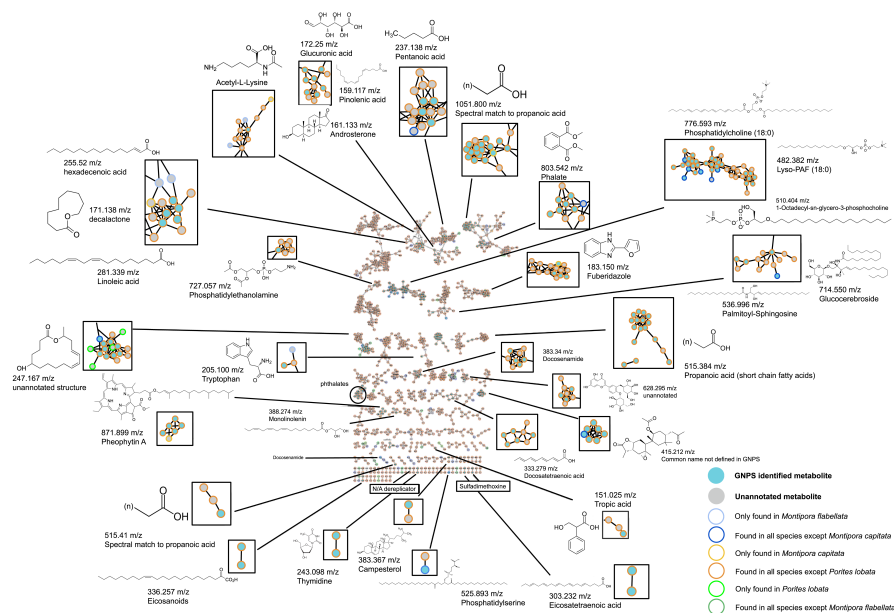


Figure 2. Blue nodes highlight level-three annotations in the GNPS molecular network of the coral assemblage. Gray nodes represent molecules without spectral matches to the GNPS database. Light blue node borders represent molecules only found in *M. flabellata* (blue rice coral). Dark blue node borders represent molecules found in all species except *M. capitata*. Light orange nodes represent molecules only found in *M. capitata* (brown rice coral). Dark orange nodes represent molecules found in all species except *P. lobata* (lobe coral). Light green borders represent molecules found only in *P. lobata*. Dark green borders are found in all species except *M. flabellata*. The network is estimated to have a 1% FDR [44]. Mass spectrometry in this experiment cannot differentiate isomeric structures, including regional, positional, and stereoisomers.

The putatively annotated metabolome of molecules shared among the different sampled coral species include long and short chain fatty acids, steroids, aromatics, sugars, phospholipids, nucleosides, amino acids, chlorophyll, a pesticide, and three unlabeled but structurally defined cyclic compounds (Figure 2). The annotated metabolome is considered putative, at level two or three according to the metabolomics consortium, as they have not been confirmed using synthetic standards or isolated and verified using other means. Using the recent false discovery rate (FDR) estimation method, the FDR is estimated to be 1% [44,45]. Fatty acids include hexadienoic acid, linoleic acid, pinolenic acid, docosenamides, docosatetraenoic acid, docosatetraenoic acid, eicosanoids, monolinolein, pentanoic acid, and propanoic acid. Steroids include androsterone and campesterol. Sugar constituents include glucuronic acid and glucocerebroside. Phospholipids include phosphatidylethanolamine, phosphatidylcholine, lyso-PAF, 1-octadecyl-sn-glycero-3-phosphocholine, palmitoyl-sphingosine, and phosphatidylserine. Thymidine nucleoside and decalactone were also annotated, as well as a pesticide known as fuberidazole. A degradation product of chlorophyll was annotated as pheophytin A. Amino acids acetyl-L-

lysine and tryptophan were annotated. Four clusters with m/z values of 628.295, 415.212, and 247.167 were annotated only by structure.

3.2. Microbiome Characterization

Closed-reference OTUs were used to characterize the microbiome of the sampled coral assemblage to family-level classification. Relative abundances of OTUs were visualized against all samples (Figure A2 shows a bacterial phyla-level summary). The top 10 most abundant bacterial families present across the coral community in descending order are as follows: *Rhodobacteraceae*, *Piscirickettsiaceae*, *Verrucomicrobiaceae*, *Hyphomicrobiaceae*, *Endozoicimonaceae*, *Pirellulaceae*, bacteria in the order *Stramniopiles*, *koll13*, *Erythrobacteraceae*, and *Clostridiaceae* (Figure 3). Bacteria from these families were found in all samples, including the water column. *Porites lobata* tissues appear to be dominated by the family *Endozoicimonaceae*, making up nearly 90% of the microbiome composition. *Montipora* tissues of both species consisted of a more diverse microbiome, with the family *Rhodobacteraceae* having the largest relative abundance.

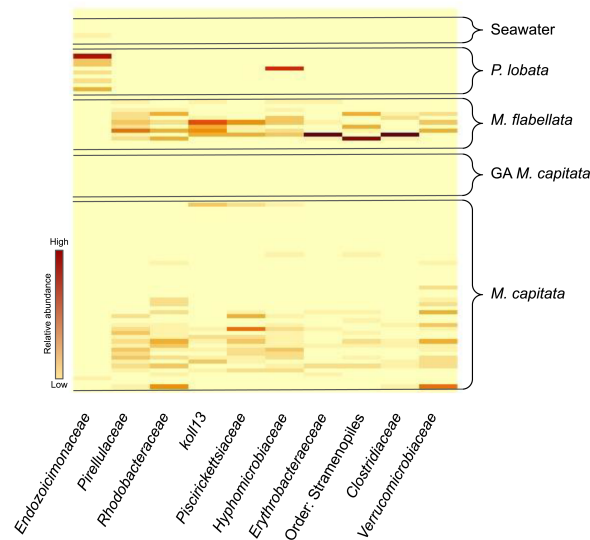


Figure 3. A taxonomic inventory of the top 10 bacterial families found in individual coral colonies comprising the Hawaiian coral assemblage and seawater at Wai’ōpae.

3.3. Metabolomic and Microbial Diversity

Metabolomic diversity (H) was significantly lower (PERMANOVA, $p < 0.001$) in *P. lobata* compared to both species of *Montipora*. Metabolomic diversity (H) was also lower in GA-affected *M. capitata* tissue compared to healthy tissues of and *M. flabellata*. Significant differences in the microbial diversity (H) were found when comparing diversity (H) among all sampled corals (Figure 4). GA-affected *M. capitata* tissue had significantly less microbial diversity when compared to healthy *M. flabellata* and *M. capitata* tissue (PERMANOVA, $p < 0.05$). Similarly, *P. lobata* tissue had significantly less microbial diversity than *M. flabellata* and *M. capitata* tissue (PERMANOVA, $p < 0.001$).

A principal coordinate analysis (PCoA) using Bray–Curtis values of dissimilarity was conducted to identify patterns among the groups of coral tissue (*M. capitata*, *M. flabellata*, and *P. lobata*). The ordination plots provide evidence of clusters, which are also supported by the PERMANOVA analysis described above (Figure 5).

Random forest classification was used to identify features that describe the metabolome and microbiome species variation with an out-of-bag (OOB) error of 0.0056 and 0.362, respectively. Although random forest provides an inventory of up to “species-level” (defined as 97% OTUs) microbial features that describe microbiome variation, the only annotated discriminatory metabolite feature was a 1-octadecyl-sn-glycero-3-phosphocholine within

the top 15 features among the sample coral species. Additionally, random forest made it possible to identify features that describe variation between GA-affected *M. capitata* tissue and healthy *M. capitata* tissue with an OOB error of 0.149 for microbiome datasets and 0.350 for metabolomic datasets. The top microbial taxonomy feature that appears to be absent in diseased tissue and present in healthy tissue is classified as a cyanobacteria belonging to the order of Stramenopiles. The top three molecular features that describe the variance between healthy and disease tissue are 226.191 *m/z*, 455.340 *m/z*, and 412.263 *m/z*. None of the top 15 features were identifiable via GNPS.

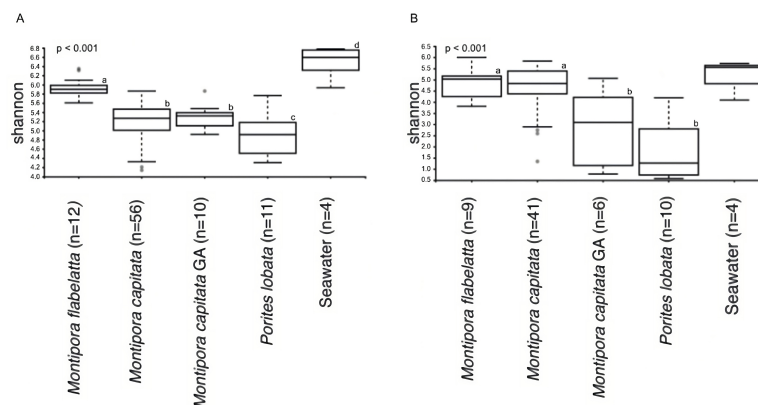


Figure 4. Differences in median (interquartile range (IQR)) molecular (A) and microbial (B) beta-diversity found in the Hawaiian coral assemblage determined by Adonis (PERMANOVA) tests on LC-MS/MS and 16S OTU feature tables. Lower case letters indicate significant groupings and points indicate outliers.

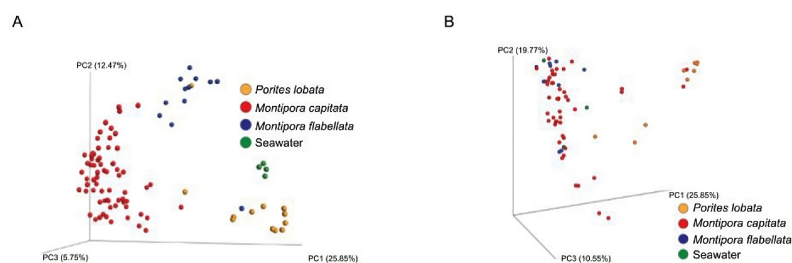


Figure 5. PCoA Bray–Curtis ordination plots that describe the metabolome (A) and the microbiome (B) of Hawaiian coral assemblage.

The top features identified from random forest analysis that describe the difference in molecular profiles between GA-affected tissue and healthy *M. capitata* tissue were also visualized in the ‘ili 3D cartography platform (Figure A3). Pheophorbide abundances were visualized and identified. Cyanobacteria of the order of Stramenopiles were mapped onto the 3D coral assemblage at each sample location to visualize the higher abundance at all sample locations compared to GA-affected tissue. Similarly, pheophorbide abundances in *M. capitata* were undetectable on GA-affected sample site locations when visualized with the ‘ili platform but present in other sites in tissue distal to *M. capitata* GA. A fully interactive visualization can be viewed on the ‘ili platform interface for the metabolome (see Data Availability).

4. Discussion

This study used an innovative 3D cartography approach to conduct a quantitative and visual characterization of the molecular profiles associated with an assemblage of Hawaiian corals. Differences in the composition and diversity of microbial and metabolomic profiles among *M. capitata*, *M. flabellata*, *P. lobata*, and GA-affected *M. capitata* coral tissue were

identified, including significant differences in the microbial and metabolomic signatures among the three coral species and between healthy and diseased tissues. Integrating genomic and metabolomic data into a 3D cartographic platform provides a powerful tool for visualizing the molecular profiles of corals on the physical reefscape created by coral colonies.

Identifying and visualizing the distribution of specific compounds within the coral tissue provides useful insight for understanding the biological implications of interference competition between coral colonies and the impacts of disease on the molecular composition of coral tissue. Sterols, the family to which the level-3 annotation campesterol belongs, have been previously found in tissue tumors and appear to be in high abundance in one of the GA-affected tissues [46]. The 3D visualization of the Wai'ōpae coral assemblage illustrates the distribution of this molecule between healthy and GA-affected tissue within the same *M. capitata* colony (Figure A3). Considering that the biology and ecology of coral diseases are still poorly understood, it is valuable to be able to search for molecules known to be associated with other animal diseases to improve the characterization of conditions affecting corals and visually assess their distributions within a coral colony [47].

Ubiquitous fatty acid and phospholipid molecules detected within the metabolome (Figure 2) of the Wai'ōpae coral assemblage are consistent with previously identified primary metabolites in scleractinian corals, soft coral, sponges, and dinoflagellates. Although lipid-based immune response pathways have been identified in marine metazoans, it remains unclear how these signaling molecules are selectively expressed in the current model [48–50].

No significant molecular differences were detected among the healthy coral tissue of separate *M. capitata* colonies, yet tissue affected by the GA disease exhibited significantly decreased molecular diversity (Figure 2). The observation suggests that a decrease in molecule abundance within GA-affected tissue could potentially decrease metabolic activity in the organism. Microbial diversity was found to be significantly lower in *P. lobata* than the other sampled coral species (Figures 2 and 3) and mirrors previous studies that found lower bacterial diversity across *Porites* coral species in other locations [5,51]. The lower microbial diversity found in the GA-affected tissue is also consistent with many microbial studies investigating the health of organisms in an array of environmental and ecological settings [52–54]. The significant decrease in diversity of both microbial and molecular features in GA-affected *M. capitata* and *P. lobata* tissue highlights the need for further research using these techniques to determine whether molecular profiles can serve as biomarkers for discriminating among coral species and health states.

A derivative of chlorophyll, pheophorbide, was distributed throughout the sampled coral assemblage, but was absent from GA-affected *M. capitata* tissue. This finding highlights the potential reduction in photosynthetic activity occurring in GA-affected tissue in relation to healthy tissue [20]. This finding supports the previous studies showing that GA has detrimental impacts on the organism's overall metabolism as the light-harvesting symbiotic microorganisms within coral tissue provide much needed nutrients for the host [55,56]. It is unclear whether the lack of photosynthesis contributes to, or is a result of, the diseased tissue, but our findings support prior research indicating a distinct photophysiological reduction in coral tissue affected by this disease [20].

Algal DNA was detected on several coral samples, which may result from chloroplast matches to the 16S rRNA gene sequence. Although some have viewed chloroplast contamination as a problem, the 3D visualizations in this study allows for visual confirmation that increased amounts of microboring algae are present within GA-affected tissue (Figure 6) [57,58]. Previous studies have investigated the relationship of turf algae growth on GA tissue at Wai'ōpae and found growth to occur on both diseased and healthy tissue [58,59]. The detection of *Ulvophyceae* suggests that this algae has found an opportunity to infiltrate colony defense and begin algal turf succession on live coral tissue. Other bacterial families have also been identified as key descriptors of the variance between healthy and diseased tissue. Although accumulations of *Rhodobacteraceae* have been associated with

coral disease in other parts of the world, levels of *Rhodobacteraceae* and overall bacterial diversity were lower in GA-affected corals [60,61].

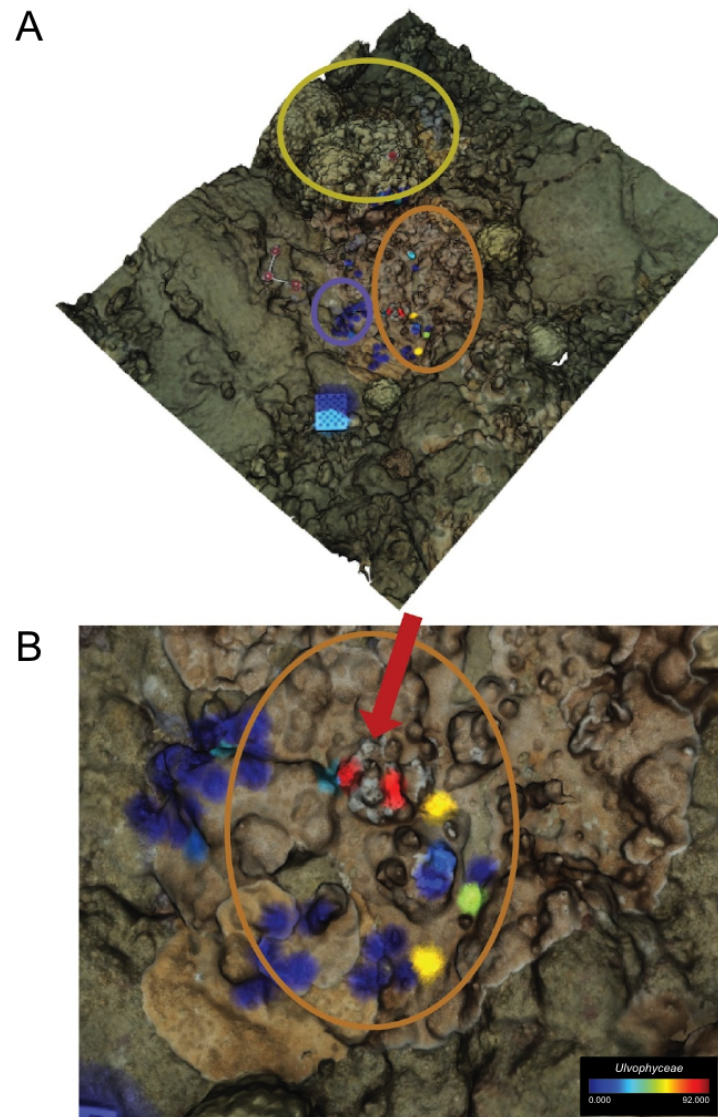


Figure 6. *Ulvophyceae* detection across coral assemblage. *P. lobata* is highlighted with a yellow circle, *M. capitata* is highlighted by an orange circle, and *M. flabellata* is highlighted with a purple circle (A). White colored tissue of GA affected *M. capitata* has a higher abundance of *Ulvophyceae* than healthy tissue of the same *M. capitata* colony (B).

5. Conclusions

As reef communities around the world exhibit declines due to anthropogenic disturbances and disease, it is critical to integrate innovative technologies to improve our understanding of the biological underpinnings that drive the ecology of these valuable coral reef ecosystems. Combining molecular and microbial profiling with 3D cartography enabled this study to create transformative visualizations to couple complex molecular datasets with high-resolution 3D reconstructions of the sampled coral colonies that can be used to identify patterns and associations that are less apparent in traditional 2D representations. This technique allows researchers to “see” patterns in molecular profiles on the physical reefscape used for sampling, which provides critical insight into the biological mechanisms associated with competition and disease. This approach can be applied to other sites to work toward detecting and characterizing molecular signatures associated

with healthy, stressed, and diseased coral tissue. Identifying molecular biomarkers of stress and disease can enhance conservation strategies aimed at protecting coral reef ecosystems.

Author Contributions: Conceptualization, C.A.K. and J.H.R.B.; Methodology, C.A.K., K.S. and L.M.K.; Software, J.H.R.B. and C.A.K.; Formal Analysis, C.A.K. and J.W.P.N.III; Investigation, C.A.K. and J.W.P.N.III; Data Curation, C.A.K., J.W.P.N.III and J.H.R.B.; Writing—Original Draft Preparation, C.A.K.; Writing—Review and Editing, C.A.K., J.H.R.B., J.W.P.N.III, K.S. and L.M.K.; Visualization, C.A.K. and J.W.P.N.III; Supervision, C.A.K. and J.H.R.B.; Project Administration, C.A.K.; Funding Acquisition, C.A.K. and J.H.R.B. All authors have read and agreed to the published version of the manuscript.

Funding: This work was partially supported by the SIO PIER fellowship awarded to C.A. Kapon. Funding and equipment were also provided to J.H.R. Burns through support by the National Science Foundation under Center for Research Excellence in Science and Technology (CREST), numbers 08332, 1345247, CREST-PRF Award No. 1720706, and Award No. 2149133, RII Track-1: Change Hawai'i: Harnessing the Data and Revolution for Island Resilience. Funding was also provided to J.H.R. Burns to support this study from Hawai'i EPSCoR (NSF award number 1557349). Any opinions, findings, and conclusions or recommendations expressed in this material are those of the author(s) and do not necessarily reflect the views of the National Science Foundation.

Data Availability Statement: The .mzXML files are openly available on the [MassIVE database](#) under accession numbers MSV000080243 and MSV000080242 (accessed 26 September 2023). Fastq files can be viewed on the [European Nucleotide Archive](#) (accessed 26 September 2023). Metabolome and microbiome visualizations on a 3D model of the coral assemblage can be viewed on the ['ili platform](#) (accessed 26 September 2023)

Acknowledgments: The authors would like to acknowledge the following for their roles and contributions to this project: Gail Ackermann for organization and management of metadata, Gregg Humphreys for completing DNA extraction and 16s rRNA sequencing, Rob Knight and Pieter Dorrestein for providing lab resources at the University of California San Diego for 16s rRNA sequencing and metabolomic profiling, and Misaki Takabayashi for lab space at the University of Hawai'i at Hilo.

Conflicts of Interest: The authors declare no conflict of interest.

Appendix A

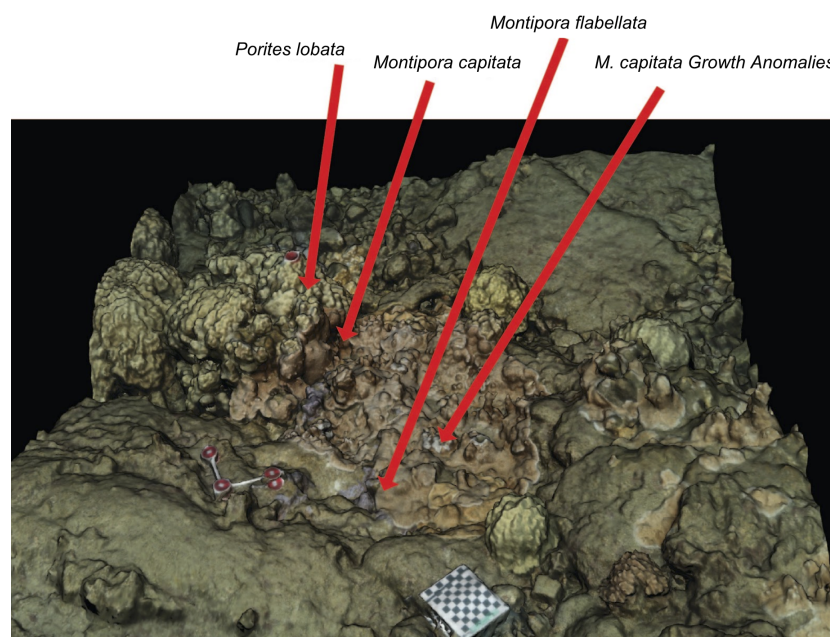


Figure A1. Sampling sites of the Wai'ōpae coral assemblage, composed of *Montipora capitata*, *Montipora flabellata*, *Porites lobata*, and *M. capitata* growth anomalies.

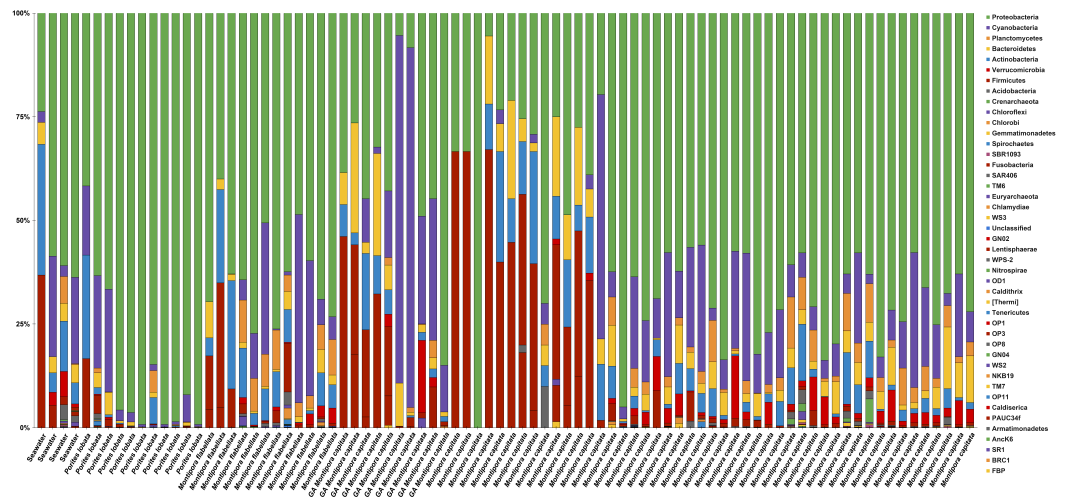


Figure A2. A taxonomic summary of all bacterial phyla found in samples of *M. capitata*, *M. flabellata*, and *P. lobata* colonies sampled from Wai'ōpae, Hawai'i.

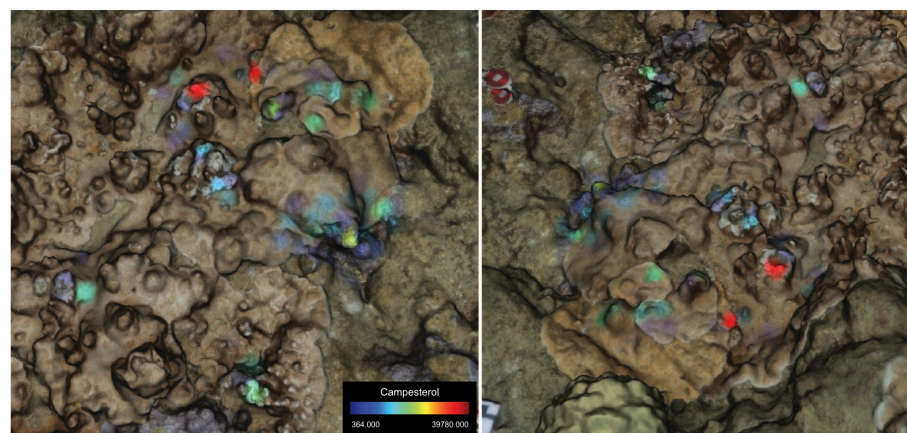


Figure A3. Spatial distribution of campesterol molecules in diseased tissue of *M. capitata* of the Wai'ōpae coral assemblage.

References

1. Lamb, J.B.; Willis, B.L.; Fiorenza, E.A.; Couch, C.S.; Howard, R.; Rader, D.N.; True, J.D.; Kelly, L.A.; Ahmad, A.; Jompa, J.; et al. Plastic waste associated with disease on coral reefs. *Science* **2018**, *359*, 460–462. [\[CrossRef\]](#)
2. Roche, R.C.; Williams, G.J.; Turner, J.R. Towards developing a mechanistic understanding of coral reef resilience to thermal stress across multiple scales. *Curr. Clim. Change Rep.* **2018**, *4*, 51–64. [\[CrossRef\]](#)
3. McDevitt-Irwin, J.M.; Baum, J.K.; Garren, M.; Vega Thurber, R.L. Towards developing a mechanistic understanding of coral reef resilience to thermal stress across multiple scales. *Front. Mar. Sci.* **2017**, *4*, 262. [\[CrossRef\]](#)
4. Rohwer, F.; Breitbart, M.; Jara, J.; Azam, F.; Knowlton, N. Diversity of bacteria associated with the Caribbean coral *Montastraea franksi*. *Coral Reefs* **2001**, *20*, 85–91.
5. Rohwer, F.; Seguritan, V.; Azam, F.; Knowlton, N. Diversity and distribution of coral-associated bacteria. *Mar. Ecol. Prog. Ser.* **2002**, *243*, 1–10. [\[CrossRef\]](#)
6. Bourne, D.G.; Garren, M.; Work, T.M.; Rosenberg, E.; Smith, G.W.; Harvell, C.D. Microbial disease and the coral holobiont. *Trends Microbiol.* **2009**, *17*, 554–562. [\[CrossRef\]](#)
7. Gordon, B.R.; Leggat, W. Symbiodinium-invertebrate symbioses and the role of metabolomics. *Mar Drugs* **2010**, *8*, 2546–2568. [\[CrossRef\]](#)
8. Costa-Lotufo, L.V.; Carnevale-Neto, F.; Trindade-Silva, A.E.; Silva, R.R.; Silva, G.G.Z.; Wilke, D.V.; Pinto, F.C.L.; Sahn, B.D.B.; Jimenez, P.C.; Mendonça, J.N.; et al. Chemical profiling of two congeneric sea mat corals along the Brazilian coast: Adaptive and functional patterns. *Chem. Commun.* **2018**, *54*, 1952–1955. [\[CrossRef\]](#)
9. Sogin, E.M.; Putnam, H.M.; Anderson, P.E.; Gates, R.D. Metabolomic signatures of increases in temperature and ocean acidification from the reef-building coral, *Pocillopora damicornis*. *Metabolomics* **2016**, *12*, 71. [\[CrossRef\]](#)

10. Hartmann, A.C.; Petras, D.; Quinn, R.A.; Protsyuk, I.; Archer, F.I.; Ransome, E.; Williams, G.J.; Bailey, B.A.; Vermeij, M.J.A.; Alexandrov, T.; et al. Meta-mass shift chemical profiling of metabolomes from coral reefs. *Proc. Natl. Acad. Sci. USA* **2017**, *114*, 11685–11690. [[CrossRef](#)]
11. McClanahan, T.R.; Donner, S.D.; Maynard, J.A.; MacNeil, M.A.; Graham, N.A.J.; Maina, J.; Baker, A.C.; Alemu I, J.B.; Beger, M.; Campbell, S.J.; et al. Prioritizing key resilience indicators to support coral reef management in a changing climate. *PLoS ONE* **2012**, *7*, e42884. [[CrossRef](#)]
12. Bythell, J.; Pan, P.; Lee, J. Three-dimensional morphometric measurements of reef corals using underwater photogrammetry techniques. *Coral Reefs* **2001**, *20*, 193–199.
13. Leon, J.X.; Roelfsema, C.M.; Saunders, M.I.; Phinn, S.R. Measuring coral reef terrain roughness using ‘Structure-from-Motion’ close-range photogrammetry. *Geomorphology* **2015**, *242*, 21–28. [[CrossRef](#)]
14. Burns, J.; Delparte, D.; Gates, R.D.; Takabayashi, M. Integrating structure-from-motion photogrammetry with geospatial software as a novel technique for quantifying 3D ecological characteristics of coral reefs. *PeerJ* **2015**, *3*, e1077. [[CrossRef](#)]
15. Burns, J.H.R.; Delparte, D.; Kapon, L.; Belt, M.; Gates, R.D.; Takabayashi, M. End of the chain? Rugosity and fine-scale bathymetry from existing underwater digital imagery using structure-from-motion (SfM) technology. *Coral Reefs* **2015**, *35*, 889–894.
16. Storlazzi, C.D.; Dartnell, P.; Hatcher, G.A.; Gibbs, A.E. Assessing the impact of acute disturbances on the structure and composition of a coral community using innovative 3D reconstruction techniques. *Methods Oceanogr.* **2015**, *15*, 49–59.
17. Protsyuk, I.; Melnik, A.V.; Nothias, L.F.; Rappez, L.; Phapale, P.; Aksenov, A.A.; Bouslimani, A.; Ryazanov, S.; Dorrestein, P.C.; Alexandrov, T. 3D molecular cartography using LC-MS facilitated by Optimus and ‘ili software. *Nat. Protoc.* **2018**, *13*, 134–154. [[CrossRef](#)]
18. Townsley, S.J.; Lamarr, T.; Trott, E. A preliminary report of the rehabilitation of the littoral marine community on a new lava flow at Kapoho, Hawai‘i. *Ecology* **1962**, *43*, 728–730. [[CrossRef](#)]
19. Burns, J.H.R.; Rozet, N.K.; Takabayashi, M. Morphology, severity, and distribution of growth anomalies in the coral, *Montipora capitata*, at Wai‘ōpae, Hawai‘i. *Coral Reefs* **2011**, *30*, 819–826. [[CrossRef](#)]
20. Burns, J.H.R.; Gregg, T.M.; Takabayashi, M. Does coral disease affect symbiodinium? Investigating the impacts of growth anomaly on symbiont photophysiology. *PLoS ONE* **2013**, *8*, e72466. [[CrossRef](#)]
21. Spies, N.P.; Takabayashi, M. Expression of galaxin and oncogene homologs in growth anomaly in the coral *Montipora capitata*. *Dis. Aquat. Organ.* **2013**, *104*, 249–256. [[CrossRef](#)]
22. Burns, J.H.R.; Alexandrov, T.; Ovchinnikova, K.; Gates, R.D.; Takabayashi, M. Data for spatial analysis of growth anomaly lesions on coral colonies using 3D reconstruction techniques. *Data Brief* **2016**, *9*, 460–462. [[CrossRef](#)]
23. Little, M.; George, E.E.; Arts, M.G.I.; Shivak, J.; Benler, S.; Huckeba, J.; Quinlan, Z.A.; Boscaro, V.; Mueller, B.; Güemes, A.G.C.; et al. Three-dimensional molecular cartography of the Caribbean reef-building coral *Orbicella faveolata*. *Front. Mar. Sci.* **2021**, *8*, 627724. [[CrossRef](#)]
24. Li, X.Q.; Chen, Z.A.; Zhang, L.T.; Jia, D. Construction and accuracy test of a 3D model of non-metric camera images using Agisoft PhotoScan. *Procedia Environ. Procedia Environ. Sci.* **2016**, *36*, 184–190.
25. Chen, Y.; Liu, H. Geomagic software for multi-sensor metrology systems. *Sens. Rev.* **2007**, *27*, 1–19.
26. Marotz, C.; Schwartz, T.; Thompson, L.; Humphrey, G.; Gogul, G.; Gaffney, J.; Amir, A.; Knight, R. Earth Microbiome Project (EMP) high throughput (HTP) DNA extraction protocol. *BioTechniques* **2017**, *62*, 290–293. [[CrossRef](#)]
27. Gilbert, J.A.; Meyer, F.; Jansson, J.; Gordon, J.; Pace, N.; Tiedje, J.; Ley, R.; Fierer, N.; Field, D.; Kyrpides, N.; et al. The Earth Microbiome Project: Meeting report of the “1st EMP meeting on sample selection and acquisition” at Argonne National Laboratory October 6th 2010. *Sens. Rev.* **2010**, *3*, 249–253. [[CrossRef](#)]
28. Wang, M.; Carver, J.J.; Phelan, V.V.; Sanchez, L.M.; Garg, N.; Peng, Y.; Nguyen, D.D.; Watrous, J.; Kapon, C.A.; Luzzatto-Knaan, T.; et al. Sharing and community curation of mass spectrometry data with Global Natural Products Social Molecular Networking. *Nat. Biotechnol.* **2016**, *34*, 828–837. [[CrossRef](#)]
29. Xia, J.; Sinelnikov, I.V.; Han, B.; Wishart, D.S. MetaboAnalyst 3.0—making metabolomics more meaningful. *Nucleic Acids Res.* **2015**, *43*, W251–W257. [[CrossRef](#)]
30. Olivon, F.; Grelier, G.; Roussi, F.; Litaudon, M.; Touboul, D. MZmine 2 Data-Preprocessing to enhance molecular networking reliability. *Anal. Chem.* **2017**, *89*, 7836–7840. [[CrossRef](#)]
31. Caporaso, J.G.; Kuczynski, J.; Stombaugh, J.; Bittinger, K.; Bushman, F.D.; Costello, E.K.; Fierer, N.; Peña, A.G.; Goodrich, J.K.; Gordon, J.I.; et al. QIIME allows analysis of high-throughput community sequencing data. *Nat. Methods* **2010**, *7*, 335–336. [[CrossRef](#)]
32. Vázquez-Baeza, Y.; Pirrung, M.; Gonzalez, A.; Knight, R. EMPeror: A tool for visualizing high-throughput microbial community data. *Gigascience* **2013**, *2*, 16. [[CrossRef](#)]
33. Yeung, N.; Cline, M.S.; Kuchinsky, A.; Smoot, M.E.; Bader, G.D. Exploring biological networks with Cytoscape software. *Bioinformatics* **2018**, *23*, 8–13. [[CrossRef](#)]
34. Shannon, P.; Markiel, A.; Ozier, O.; Baliga, N.S.; Wang, J.T.; Ramage, D.; Amin, N.; Schwikowski, B.; Ideker, T. Cytoscape: A software environment for integrated models of biomolecular interaction networks. *Genome Res.* **2003**, *13*, 2498–2504. [[CrossRef](#)]

35. Bruno, F.; Gallo, A.; De Filippo, F.; Muzzupappa, M.; Petriaggi, B.D.; Caputo, P. 3D documentation and monitoring of the experimental cleaning operations in the underwater archaeological site of Baia (Italy). *Digit. Herit. Int. Congr. (DigitalHeritage)* **2013**, *1*, 105–112.
36. McCarthy, J.; Benjamin, J. Multi-image Photogrammetry for Underwater Archaeological Site Recording: An Accessible, Diver-Based Approach. *J. Marit. Archaeol.* **2014**, *9*, 95–114. [[CrossRef](#)]
37. Kersten, T.P.; Lindstaedt, M. Automatic 3D object reconstruction from multiple images for architectural, cultural heritage and archaeological applications using open-source software and web services. *Photogramm. Fernerkun.* **2012**, 727–740. [[CrossRef](#)]
38. Gordon, B.R.; Leggat, W.; Motti, C.A. Extraction protocol for nontargeted NMR and LC-MS metabolomics-based analysis of hard coral and their algal symbionts. *Methods Mol. Biol.* **2013**, *1055*, 129–147.
39. Caporaso, J.G.; Lauber, C.L.; Walters, W.A.; Berg-Lyons, D.; Huntley, J.; Fierer, N.; Owens, S.M.; Betley, J.; Fraser, L.; Bauer, M.; et al. Ultra-high-throughput microbial community analysis on the Illumina HiSeq and MiSeq platforms. *ISME J.* **2012**, *6*, 1621–1624. [[CrossRef](#)]
40. Dixon, P. VEGAN, a package of R functions for community ecology. *J. Veg. Sci.* **2003**, *14*, 927–930. [[CrossRef](#)]
41. Speiser, J.L.; Miller, M.E.; Tooze, J.; Ip, E. A comparison of random forest variable selection methods for classification prediction modeling. *Expert Syst. Appl.* **2019**, *134*, 93–101. [[CrossRef](#)]
42. Xia, J.; Wishart, D.S. Metabolomic data processing, analysis, and interpretation using MetaboAnalyst. *Curr. Protoc. Bioinform.* **2011**, *34*, 4.10.1–14.10.48. [[CrossRef](#)]
43. Sumner, L.W.; Amberg, A.; Barrett, D.; Beale, M.H.; Beger, R.; Daykin, C.A.; Fan, T.W.M.; Fiehn, O.; Goodacre, R.; Griffin, J.L.; et al. Proposed minimum reporting standards for chemical analysis. *Metabolomics* **2007**, *3*, 211–221. [[CrossRef](#)]
44. Mohimani, H.; Gurevich, A.; Mikheenko, A.; Garg, N.; Nothias, L.F.; Ninomiya, A.; Takada, K.; Dorrestein, P.C.; Pevzner, P.A. Dereplication of peptidic natural products through database search of mass spectra. *Nat. Chem. Biol.* **2017**, *13*, 30–37. [[CrossRef](#)]
45. Walzthoeni, T.; Claassen, M.; Leitner, A.; Herzog, F.; Bohn, S.; Förster, F.; Beck, M.; Aebersold, R. False discovery rate estimation for cross-linked peptides identified by mass spectrometry. *Nat. Methods* **2012**, *9*, 901–903. [[CrossRef](#)]
46. Yamashiro, H.; Oku, H.; Onaga, K.; Iwasaki, H.; Takara, K. Coral tumors store reduced level of lipids. *J. Exp. Mar. Biol.* **2001**, *265*, 171–179. [[CrossRef](#)]
47. Richardson, L.L. Coral diseases: What is really known? *Trends Ecol. Evol.* **1998**, *13*, 438–443. [[CrossRef](#)]
48. Garg, N.; Kapon, C.A.; Lim, Y.W.; Koyama, N.; Vermeij, M.J.; Conrad, D.; Rohwer, F.; Dorrestein, P.C. Mass spectral similarity for untargeted metabolomics data analysis of complex mixtures. *Int. J. Mass Spectrom.* **2015**, *377*, 719–727. [[CrossRef](#)]
49. Quinn, R.A.; Vermeij, M.J.; Hartmann, A.C.; Galtier d’Auriac, I.; Benler, S.; Haas, A.; Quistad, S.D.; Lim, Y.W.; Little, M.; Sandin, S.; et al. Metabolomics of reef benthic interactions reveals a bioactive lipid involved in coral defense. *Proc. Royal Soc.* **2016**, *283*, 20160469.
50. Mannocho-Russo, H.; Swift, S.O.I.; Nakayama, K.K.; Wall, C.B.; Gentry, E.C.; Panitchpakdi, M.; Caraballo-Rodriguez, A.M.; Aron, A.T.; Petras, D.; Dorrestein, K.; et al. Microbiomes and metabolomes of dominant coral reef primary producers illustrate a potential role for immunolipids in marine symbioses. *Commun. Biol.* **2023**, *6*, 896. [[CrossRef](#)]
51. Speck, M.D.; Conachie, S.P. Widespread Oceanospirillaceae bacteria in *Porites* spp. *J. Mar. Sci.* **2012**, *2012*, 746720. [[CrossRef](#)]
52. Clay, K.; Holah, J. Fungal endophyte symbiosis and plant diversity in successional fields. *Science* **1999**, *285*, 1742–1744. [[CrossRef](#)]
53. Chang, J.Y.; Antonopoulos, D.A.; Kalra, A.; Tonelli, A.; Khalife, W.T.; Schmidt, T.M.; Young, V.B. Decreased diversity of the fecal microbiome in recurrent *Clostridium difficile*-associated diarrhea. *J. Infect. Dis.* **2008**, *197*, 435–438. [[CrossRef](#)]
54. Keesing, F.; Belden, L.K.; Daszak, P.; Dobson, A.; Harvell, C.D.; Holt, R.D.; Hudson, P.; Jolles, A.; Jones, K.E.; Mitchell, C.E.; et al. Impacts of biodiversity on the emergence and transmission of infectious diseases. *Nature* **2010**, *468*, 647–652. [[CrossRef](#)]
55. Muscatine, L.; Porter, J.W. Reef Corals: Mutualistic Symbioses Adapted to Nutrient-Poor Environments. *Bioscience* **1977**, *3*, 454–460. [[CrossRef](#)]
56. Hatcher, B.G. Coral reef primary productivity: A beggar’s banquet. *Trends Ecol. Evol.* **1988**, *27*, 106–111. [[CrossRef](#)]
57. Hanshew, A.S.; Mason, C.J.; Raffa, K.F.; Currie, C.R. Minimization of chloroplast contamination in 16S rRNA gene pyrosequencing of insect herbivore bacterial communities. *J. Microbiol. Methods* **2013**, *95*, 149–155. [[CrossRef](#)]
58. Massé, A.; Domart-Coulon, I.; Golubic, S.; Duché, D.; Tribollet, A. Early skeletal colonization of the coral holobiont by the microboring *Ulvophyceae* *Ostreobium* sp. *Sci. Rep.* **2018**, *8*, 2293. [[CrossRef](#)]
59. Claar, D.C.; Takabayashi, M. The effects of growth anomaly on susceptibility of *Montipora capitata* to turf algal overgrowth. *Mar. Freshw. Res.* **2015**, *67*, 666–670. [[CrossRef](#)]
60. Roder, C.; Arif, C.; Bayer, T.; Aranda, M.; Daniels, C.; Shibl, A.; Chavanich, S.; Voolstra, C.R. Bacterial profiling of White Plague Disease in a comparative coral species framework. *ISME J.* **2014**, *8*, 31–39. [[CrossRef](#)]
61. Sunagawa, S.; DeSantis, T.Z.; Piceno, Y.M.; Brodie, E.L.; DeSalvo, M.K.; Voolstra, C.R.; Weil, E.; Andersen, G.L.; Medina, M. Bacterial diversity and White Plague Disease-associated community changes in the Caribbean coral *Montastraea faveolata*. *ISME J.* **2009**, *3*, 512–521. [[CrossRef](#)] [[PubMed](#)]

Disclaimer/Publisher’s Note: The statements, opinions and data contained in all publications are solely those of the individual author(s) and contributor(s) and not of MDPI and/or the editor(s). MDPI and/or the editor(s) disclaim responsibility for any injury to people or property resulting from any ideas, methods, instructions or products referred to in the content.